NANOSYSTEMS: PHYSICS, CHEMISTRY, MATHEMATICS, 2020, 11 (2), P. 230–236

Electrochemical investigation of hydrothermally induced $MnCo_2S_4$ nanoparticles as an electrode material for high performance supercapacitors

M. Dakshana[1], S. Meyvel[1], M. Malarvizhi[1], P. Sathya[2]

[1]Chikkaiah Naicker College, Erode-63, India

[2]Salem Sowdeswari College, Salem, India

meyvelphd@gmail.com

DOI 10.17586/2220-8054-2020-11-2-230-236

Ternary spinel $MnCo_2S_4$ spherical nanoparticles are prepared through a simple one step hydrothermal approach with precursors followed by an ion exchange reaction. The obtained spherical nanoparticles offers a high specific surface area with mesoporous structure, this aids in providing outstanding electrochemical performance with a specific capacitance of 707.77 F/g at 2 A/g and a good cyclic stability (initial capacitance of 95.15% after 10000 cycles). It offers a high energy density of 78.17 W h Kg^{-1} to satisfy the commercial needs. By the utilization of structural and electrochemical benefits, $MnCo_2S_4$ electrode establishes its significant potential in the field of energy storage system.

Keywords: electrode material, psudeocapacitor, ternary metal sulfides.

Received: 15 March 2020

Revised: 4 April 2020

1. Introduction

Electrical energy is one of the most imperative topics in recent years due to its growing demand on storage in a sustainable way [1]. Among, diverse energy conversion and storage systems, supercapacitor is a new class of electrochemical energy system known for its notable power density, long term stability, superfast charge and discharge efficacy, long cycle life and environmental favorable. Yet they suffer from a low energy density this inhibits them from commercial applications [2]. An electrode material plays a predominant role in determining the supercapacitor performance. According to the previous reported literature several active materials like transition metal oxides, metal hydroxides, metal sulfides, conductive polymers and carbon based materials are effectively studied for supercapacitor applications. Among them, metal sulfides along with mono metal sulfides and bimetal sulfides are considered as promising candidates with remarkable properties in various applications like electro catalyst in hydrogen evolution reaction and as electrode material for energy storage applications. Amid different (NiS, CoS, ZnS) mono metal sulfides, e.g., cobalt sulfides, which appear to exist in different phases, such as $Co_{1-x}S$, Co_9S_8, Co_2S_3, Co_3S_4, provide various oxidation states which enhance their supercapacitor performance but they still suffer from low conductivity, poor mechanical stability and reduced specific capacitance when prepared via conventional methods. Compared to mono metal sulfides, binary metal sulfides have attracted much research attention by their superior capacitive performance and electrochemical activity obtained by its rich redox active sites and intensified charge transfer into different metal ions [3, 4]. Recently, pseudo capacitive bimetal sulfide, e.g., $NiCo_2S_4$, $ZnCo_2S_4$, $CuCo_2S_4$, $MnCo_2S_4$, and $FeCo_2S_4$ [2] offer excellent conductivity than the oxide counterparts. Due to their sulpho spinel structure, they result in low band gap energies which promote enhanced electrical conductivity ~ 100 times superior than oxide counterparts. Moreover, the low elctronegativity of sulfur provides a stable structure by forbidding the structure expansion, hence fast electron transportation is forwarded by its reinforced mechanical flexibility [2, 3] Among various binary metal sulfides, $MnCo_2S_4$ is finely studied as one of the most promising candidates with appreciable capacitive properties and good rate capabilities in supercapacitor applications; that fact is a result of the synergetic effect of cobalt with large oxidation potential and manganese, with more electrons [2, 5, 6].

The porosity level and morphology of the prepared electrode material also plays a vital role in determining its electrochemical performance. In this work, we adopted a one-step hydrothermal approach for the successful preparation of $MnCo_2S_4$ nanoparticles as a supercapacitor electrode material endowed with nanospheres like morphology and specific capacitance of 707.77 F/g at 2 A/g, it provide a high energy density of 78.17 W h Kg^{-1} at a power density of 863.27 W Kg^{-1} they offer an outstanding cyclic stability with a notable capacitance retention of 95.15% after 10000 galvanostatic charge discharge (GCD) cycles, these results suggest that $MnCo_2S_4$ is suitable candidate for high energy density supercapacitor applications.

2. Experimental

In this simple procedure, 0.2 mmol of $Mn(NO_3)_26H_2O$ and 0.4 mmol of $Co(NO_3)_26H_2O$ were dissolved in 60 ml of distilled water under uniform stirring for 30 minutes to achieve a homogenous solution, later 0.8 mmol of C_2H_5NS (thioacetamide) as sulfur source is made to dissolve in 25 ml of ethanol and combined to the above homogenous solution in a drop wise manner, followed by steady stirring for 6 hours. Next, the end solution was transferred into a Teflon- coated stainless autoclave. The autoclave was locked and treated in a hot air oven for 24 hours at 160 °C. After the thermal treatment, the autoclave was naturally cooled down to room temperature. The resultant black precipitate was put into centrifuged (Hamilton Bell v6500 Vanguard centrifuge) at 2600 RPM for 20 minutes and washed thoroughly with deionized water and ethanol by a number of times to remove the residuals and followed by drying in a vaccum oven at 110 °C for 6 hours and finely ground and this successive formation of $MnCo_2S_4$ nanoparticles.

3. Material characterization

Philips XPERT-PRO (Cu-K$\alpha\lambda = 1.5418$ Å) instrument were utilized to analyze crystalline nature of the sample via X-Ray Diffraction (XRD) pattern. JEM-2100 (JEOL, JAPAN) was used to obtain TEM images and their associated selected area electron diffraction (SAED) patterns. The chemical state and composition of the prepared sample was examined by XPS Ultra axis instrument (Kratos Analytical). The specific surface area and porous nature of the sample was studied via nitrogen adsorption- desorption analysis using BETSORP MAX (Microtrac BEL, Japan). The electrochemical properties of the gleaned electrode were measured by the instrument CHI 660E electrochemical workstation in a three-electrode cell frame work containing 2.0M KOH electrolyte solution with a potential range 0-0.5V Vs (Ag/Agcl).

4. Framing of electrode

The as-obtained powder sample was integrated as working electrode containing 80% of prepared sample, 15% of carbon black and 5% of PVDF (Polvinylidene Fluoride). A certain amount of N-methylpyrrolidone (NMP) was added to bind as homogenous slurry, the as formed slurry was loaded on to the nickel foam (1×1 cm^2) followed by drying in vacuum oven at 80 °C for 10 hours. The mass loading of electrode/cm^2 was predicted around 1.96 mg/cm^2.

5. Results and discussion

5.1. XRD analysis

Figure 1 shows the XRD pattern of $MnCo_2S_4$. Despite the fact, there is no standard pattern for $MnCo_2S_4$, the well-defined diffraction peaks located at 2θ = 16.2, 26.6, 30.9, 31.8 and 36.3° were indexed to the (111), (220), (311), (222) and (400) planes of cubic Co_3S_4 (JCPDS card number 73-1703) [5]. This indicates that addition of Mn to cobalt sulfide does not alter the crystal structure with slight changes in the lattice parameter [2]. Hence, the obtained product was mainly composed of $MnCo_2S_4$.

5.2. XPS characterization

The existence of constituent elements and chemical state of $MnCo_2S_4$ nanostructures were determined by XPS studies. From Mn2p spectrum (Fig. 2), the peaks positioned at 653.7, 641.5 and 643.6, 654.5 eV were attributed to Mn^{2+} and Mn^{3+} respectively [7]. In order, to conform the oxidation state of Mn, the MnS Spectrum was utilized. As shown in Fig. 3, it holds a binding energy splitting width of about 6.01 eV, which fits the Mn^{2+} oxidation state [3].

Whereas the Co2p spectrum in Fig. 4 showed two spin-orbit doublets of Co^{2+} and Co^{3+} and two shake up satellites. The peak located at 795.9 eV corresponds to $Co2p_{1/2}$ with a shoulder at 801.2 eV and the peak appeared at 779.8 eV related to $Co2p_{3/2}$ with satellite peak at 784.1 eV. The presence of weak satellite peaks indicates that the majority of cobalt is Co^{3+}. The spin separation of $Co2p_{3/2}$ and $Co2p_{1/2}$ is around 15 eV due to co-existence of Co^{3+} and Co^{2+} [8]. The S2p spectrum (Fig. 5) displayed a main peak of metal-sulfur bond at 163.8 eV and shake-up satellite peak at 168.3 eV [9].

5.3. Structural analysis

TEM micrograph images (Fig. 6 and Fig. 7) of $MnCo_2S_4$ recognized the non-uniformly dispersed nanospheres resembling structure of surface of size 16–17 nm. This uncommon morphology provides sufficient open space as an electroactive surface. From the high-resolution transmission electron microscope (HRTEM) image (Fig. 8), the inter-planar distance of lattice fringes is measured as 0.321 nm that correspond to (2 2 0) crystallographic planes. These

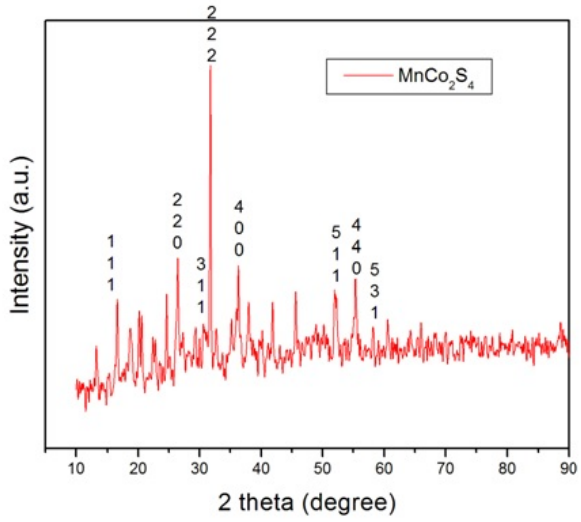

FIG. 1. X-ray diffraction pattern of $MnCo_2S_4$

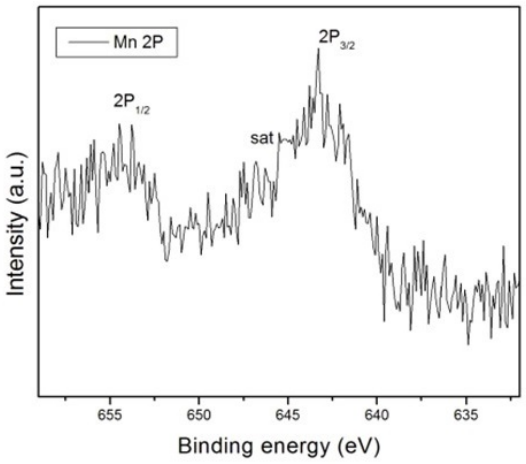

FIG. 2. XPS Spectrum of manganese element

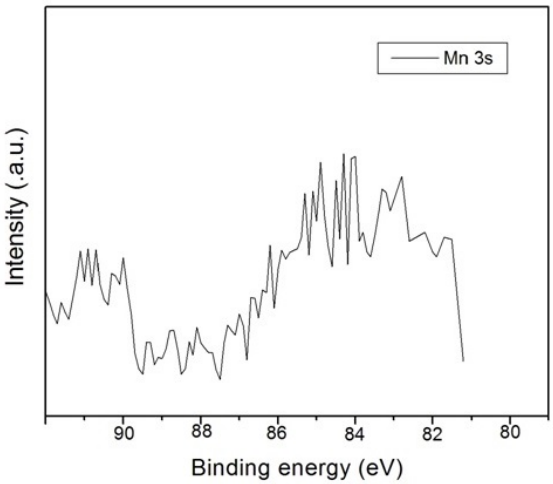

FIG. 3. Mn 3s spectrum

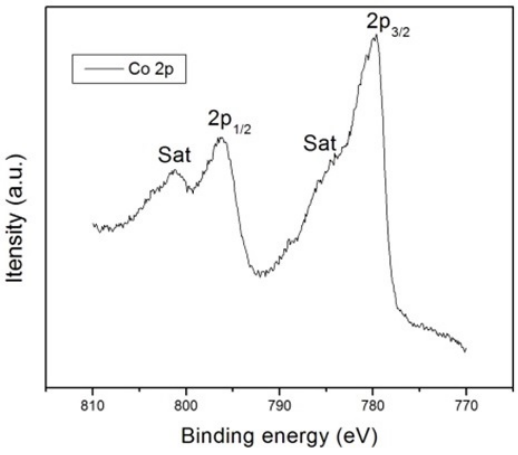

FIG. 4. XPS Spectrum of cobalt element

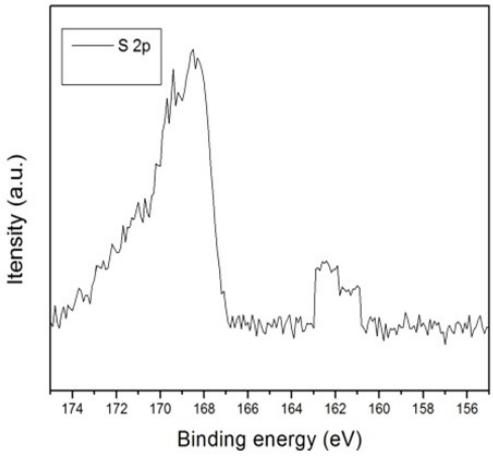

FIG. 5. XPS Spectrum of sulphur element

results are reliable with X-ray diffraction (XRD) analysis and the inset of Fig. 9, shows similar SAED which authenticates its polycrystalline nature. The EDX spectrum of the representative sample illustrated in Fig. 10 confirmed the presence of Mn, Co, and S elements.

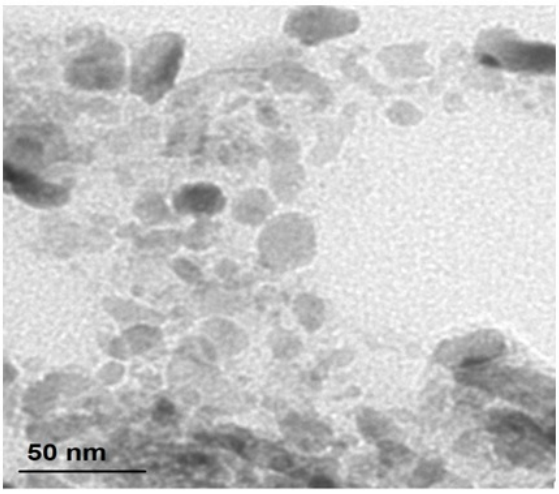

FIG. 6. TEM micrograph images of $MnCo_2S_4$

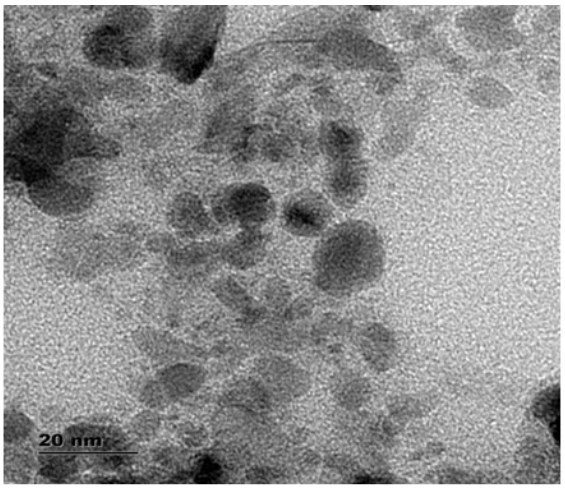

FIG. 7. TEM micrograph images of $MnCo_2S_4$

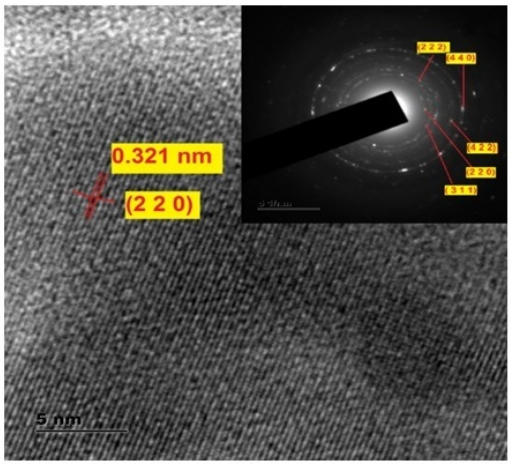

FIG. 8. SAED pattern of $MnCo_2S_4$

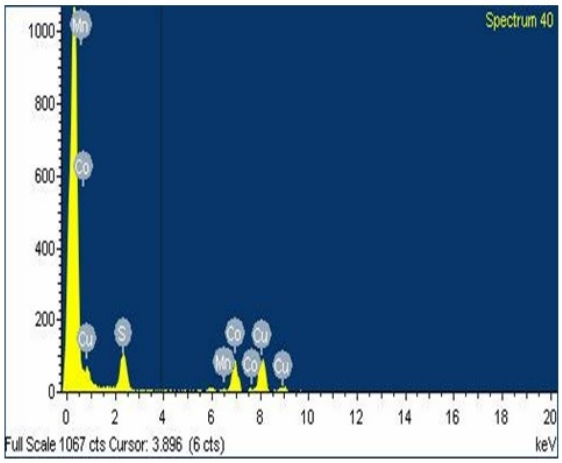

FIG. 9. EDS Spectrum of $MnCo_2S_4$

5.4. Surface area and pore size analysis

The adsorption isotherms shown in Fig. 9 are classified as type IV hysteresis loops that hold to the mesoporous structure [10] of the sample. It can be further confirmed by the Barett–Joyner–Halenda (inset of Fig. 10) pore size distribution data, the resultant pore distribution are narrow and most of the pores are mainly centered in the range of 6.95 nm. They enclose a high surface area of 73.26 m^2g^{-1} due to a typical nanosphere-like architecture. The high specific surface area and mesoporous nature of the prepared sample provides abundant electron-active sites and short diffusion path for charge transport channels this in turn improve electrochemical reactions in the redox process, and results in appreciable specific capacitance.

5.5. Electrochemical properties

5.5.1. Cyclic voltammetry studies. The electrochemical characterization was carried out in a 3-electrode system with $MnCo_2S_4$ electrode as the working electrode. Fig. 11 depicts CV curves at different scan rates, the pair of redox peaks are caused by interaction between sulphospinel materials and electrolyte ions [2, 3]. Redox peaks affirm the reversible faradaic property attributed to the pseudocapacitive behavior of the $MnCo_2S_4$ electrode. The substantial shape maintains of CV curves suggests the good redox reaction reversibility of the electrode [2], moreover, with

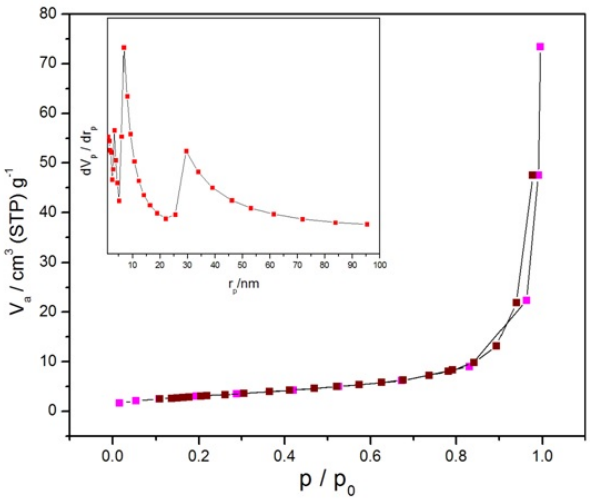

FIG. 10. N_2 sorption isotherms and differential mesopore size distribution $\Delta V/\Delta d$ plots (inset) of $MnCo_2S_4$

respect to the scan rate the anodic and cathodic peak shifts, this corresponds to the fast charge/discharge rates. The interaction between the electrode material and electrolyte ions [11, 12] are given by the following equations [3]:

$$\text{MnS+OH}^- \leftrightarrow \text{MnSOH} + e^- \tag{1}$$

$$\text{CoS+OH}^- \leftrightarrow \text{CoSOH} + e^- \tag{2}$$

$$\text{CoSOH +OH}^- = \text{CoSO+H}_2\text{O} + e^- \tag{3}$$

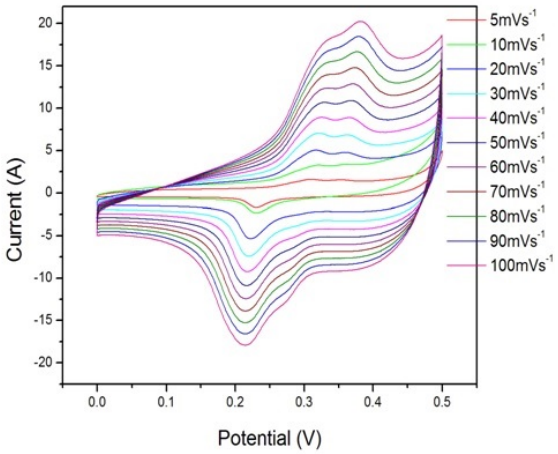

FIG. 11. CV curves of $MnCo_2S_4$ at various scan rates

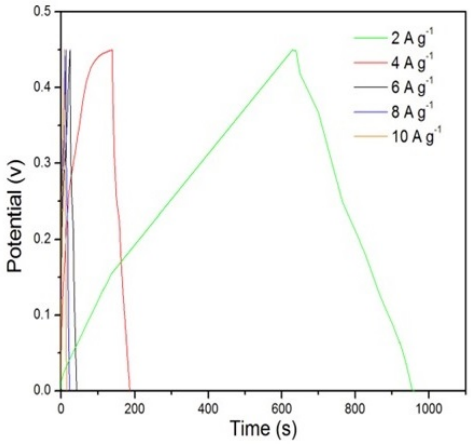

FIG. 12. Charge/Discharge curves of $MnCo_2S_4$ at various current densities

5.5.2. Galvanostatic Charge/Discharge Analysis. The pseudo capacitive property of $MnCo_2S_4$ nanoparicles were established by well-symmetric glavanostatic charge/discharge (GCD) curves (Fig. 12) at a potential window of 0.0–0.5 V with different current densities [4]. The specific capacitance is calculated using the following equation [13]:

$$c_s = \frac{l\Delta t}{m\Delta v}. \tag{4}$$

The superior specific capacitance of 707.77 F/g at 2 A/g is obtained. As shown in Fig. 13, the specific capacitance decreases as current density increases, due to minimum utilization of active material and at high discharge current densities the controlled diffusion presents its inability to maintain the redox transition completely. To determine the cycle ability, the electrodes are subjected to continuous charge/discharge cycles of 10000 cycles at a current density of 10 A/g. The structural stability is a crucial factor in evaluating the cycle ability of the electrode material. Since,

the electrode material enclose a porous nanosphere-like morphology which leads to better ionic conductivity and accessibility to reach active sites in electrode material This helps in providing capacitance retention of 95.15% after 10000 GCD cycles (Fig. 14) which is achieved by good structural stability. To satisfy its commercial needs, a Ragone plot of energy density vs. power density profile (Fig. 15) is studied and it is endowed with an appreciable energy density of 78.1 W h Kg^{-1} at a power density 863.27 W Kg^{-1}.

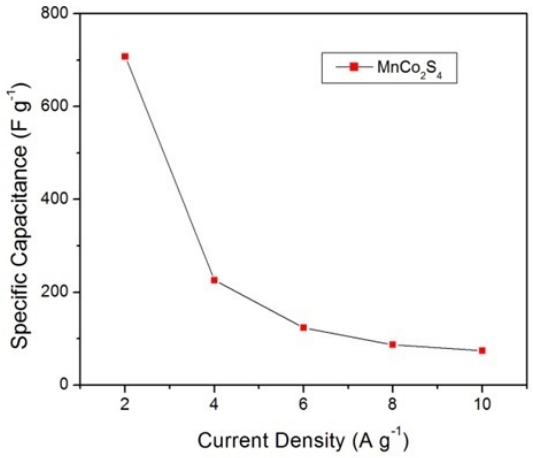

FIG. 13. Current density vs specific capacity plot of $MnCo_2S_4$

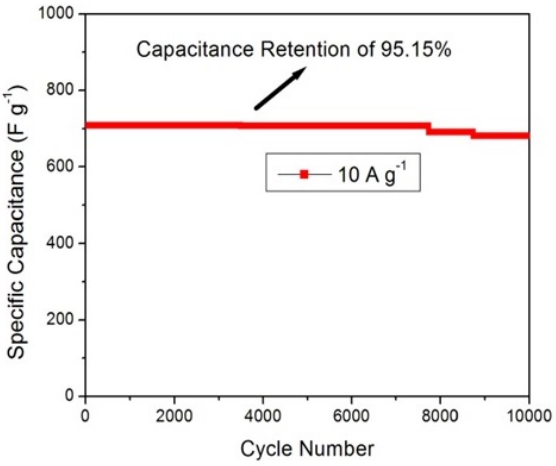

FIG. 14. Cyclic stability of $MnCo_2S_4$ electrodes at 10 Å g^{-1}

5.5.3. EIS characterization. EIS measurements were taken in defining impedance response of $MnCo_2S_4$ electrode materials in the frequency region 100 KHz – 0.01 Hz at an open-circuit potential of amplitude 5 mV and their corresponding Nyquist plot is portrayed in Fig. 16. The straight line at low frequency region specify the capacitive behavior, charge transfer resistance R_{ct} is premeditated from the semi-circle in the high frequency region, negligible semicircle indicates the very lowest charge-transfer resistances, and this improves the speedy electron transfer in the charge-discharge process leading to high-rate capability and notable supercapacitor performance [15, 16].

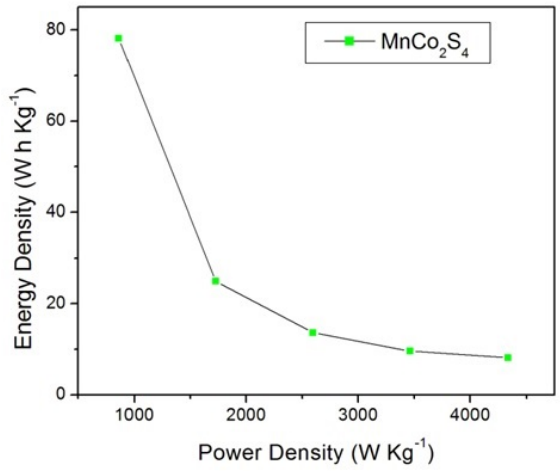

FIG. 15. Ragone plot of $MnCo_2S_4$

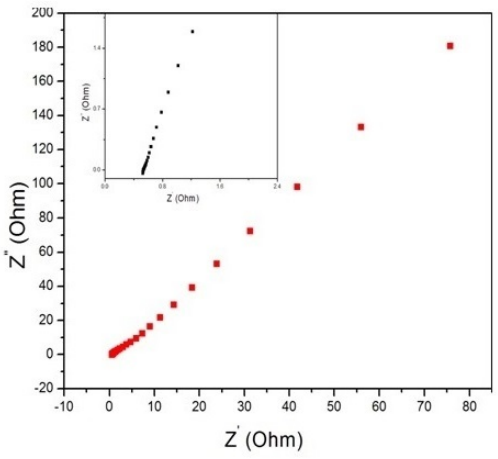

FIG. 16. EIS plot of $MnCo_2S_4$ electrode

6. Conclusion

A $MnCo_2S_4$ supercapacitor electrode with a propitious electrochemical performance was expediently fabricated using a simple one step hydrothermal method. The nanospheres like architecture of size 16–17 nm provide a highly accessible porous structure which assists superior specific capacitance of 707.77 F/g at a current density of 2 A/g; it

also has capacitance retention of 95.15% of initial capacitance after 10000 GCD cycles. The excellent performances contributed to the high surface area with mesoporous structure and low charge transfer resistance suggests that the $MnCo_2S_4$ could be utilized in fabricating high competency energy storage device.

References

[1] Bu Yuan,Yu, Xial Wang, Shuyan Song and Xiong Wen (David) Lou. Formation of onion-like $NiCo_2S_4$ particles via sequential ion-exchange for hybrid supercapacitors. *Adv. Mater. United States*, 2016, **29**, P. 1605051.

[2] Hongfei Wang, Hongfei, Zhang, Kefu, Song, Yuqing, Qiu, Jun, Wu, Juan and Yan, Lifeng. $MnCo_2S_4$ nanoparticles anchored to N- and S-codoped 3D graphene as a prominent electrode for asymmetric supercapacitors. *Carbon. United Kingdom*, 2019, **146**, P. 420–429.

[3] Elshahawy, Abdelnaby M., Li, Xin, Zhang, Hong, Hu, Yating, Ho, Kuan Hung, Guan Cao and Wang John. Controllable $MnCo_2S_4$ nanostructures for high performance hybrid supercapacitors. *J. Mater. Chem. A*, 2017, **5**, P. 7494–7506.

[4] Huang, Yunpeng, Cui, Fen, Bao, Jian, Zhao, Yan, Lian, Jiabiao, Liu, Tianxi and Li, Huaming. $MnCo_2S_4$/$FeCo_2S_4$ "lollipop" arrays on a hollow N-doped carbon skeleton as flexible electrodes for hybrid supercapacitors. *J. Mater. Chem. A*, 2019, **7**, P. 20778–20789.

[5] Liu S. and Jun S.C. Hierarchical manganese cobalt sulfide core–shell nanostructures for high-performance asymmetric supercapacitors. *J. Power Sources*, 2017, **342**, P. 629–637.

[6] Jia, Hong, Song, Yingying, Wu, Jie, Fu, Wenwen, Zhao, Jianguo and Liu, Xianming. A novel P-doped $MnCo_2S_4$ nanoneedles assembled dandelion-like structure for high performance hybrid supercapacitors. *Mater. Lett. Netherlands*, 2018, **233**, P. 55–58.

[7] Li, Wenhua, He, Lei, Zhang, Jing, Li, Bin, Chen, Qianqiao and Zhong, Qin. Anchoring spinel $MnCo_2S_4$ on carbon nanotubes as efficient counter electrodes for Quantum Dot Sensitized solar cells. *J. Phys. Chem. C.*, 2019, **123**, P. 21866–21873.

[8] Yin, Jialin, Zhang, Hao, Luo, Jiaqiu, Yao, Mengqi and Hu, Wencheng. High-boiling-point solvent synthesis of mesoporous $NiCo_2S_4$ with high specific surface area as supercapacitor electrode material. *J. Mater. Sci. Mater. Electron*, 2016, **28**, P. 2093–2099.

[9] Gong X.F., Cheng J.P., Ma K.Y., Liu F., Zhang Li and Zhang XiaoBin. Nanostructured nickel-cobalt sulfide grown on nickel foam directly as supercapacitor electrodes with high specific capacitance. *Mater. Chem. Phys.*, 2016, **173**, P. 317–324.

[10] Zhu, Tao, Zhang, Guoxiong, Hu, Tao, He, Zhenni, Lu, Yisheng, Wang, Guiqing, Guo, Haibo, Luo, Jian, Lin, Chuan and Chen, Yigang. Synthesis of $NiCo_2S_4$-based nanostructured electrodes supported on nickel foams with superior electrochemical performance. *J. Mater. Sci.*, 2015, **51**, P. 1903–1913.

[11] Atin Pramanik, Sandipan Maiti, Monjoy Sreemany, and Sourindra Mahanty. Carbon Doped $MnCo_2S_4$ Microcubes Grown on Ni Foam as High Energy Density Faradaic Electrode. *Electrochim. Acta*, 2016, **213**, P. 672–679.

[12] Silambarasan M., Padmanathan N., Ramesh P.S., Geetha D. Spinel $CuCo_2O_4$ Nanoparticles: Facile One-Step Synthesis, Optical, and Electrochemical Properties. *Mater. Res. Express*, 2016, **3**, P. 095021.

[13] Dakshana M., Meyvel S., Malarvizhi M., Sathya P., Ramesh R., Prabhu S. and Silambarasan M. Facile synthesis of $CuCo_2S_4$ nanoparticles as a faradaic electrode for high performance supercapacitor applications. *Vacuum*, 2020, **174**, P. 109218.

[14] Saravanakumar B., Ramachandran S.P., Ravi G., Ganesh V., Sakunthala A. and Yuvakkumar R. Morphology dependent electrochemical capacitor performance of $NiMoO_4$ nanoparticles. *Mater. Lett.* 2017, **209**, P. 1–4.

[15] Wen, Ping, Fan, Mingjin, Yang, Desuo, Wang, Yan, Cheng, Hualei and Wang, Jinqing. An asymmetric supercapacitor with ultrahigh energy density based on nickle cobalt sulfide nanocluster anchoring multi-wall carbon nanotubes. *J. Power Sources*, 2016, **320**, P. 28–36.

[16] Jun Pu, Tingting Wang, Haiyang Wang, Yao Tong, Chenchen Lu, Wei Kong, and Zhenghua Wang. Direct Growth of $NiCo_2S_4$ Nanotube Arrays on Nickel Foam as High-Performance Binder-Free Electrodes for Supercapacitors. *Chem Plus Chem*, 2014, **79**, P. 577–583.